FEBS Letters 586 (2012) 344–349

FEBS Letters

journal homepage: www.FEBSLetters.org

Dimerization, but not phosphothreonine binding, is conserved between the forkhead-associated domains of Drosophila MU2 and human MDC1

Shukun Luo [a,b], Keqiong Ye [b,*]

[a] College of Biological Sciences, China Agricultural University, 2 Yuanmingyuan West Road, Beijing 100094, China
[b] National Institute of Biological Sciences, 7 Science Park Road, Beijing 102206, China

ARTICLE INFO

Article history:
Received 13 January 2012
Accepted 15 January 2012
Available online 21 January 2012

Edited by Kaspar Locher

Keywords:
X-ray crystallography
DNA damage response
Forkhead-associated domain
MDC1
Molecular evolution

ABSTRACT

Mutator 2 (MU2) in *Drosophila melanogaster* has been proposed to be the ortholog of human MDC1, a key mediator in DNA damage response. The forkhead-associated (FHA) domain of MDC1 is a dimerization module regulated by *trans* binding to phosphothreonine 4 from another molecule. Here we present the crystal structure of the MU2 FHA domain at 1.9 Å resolution, revealing its evolutionarily conserved role in dimerization. As compared to the MDC1 FHA domain, the MU2 FHA domain dimerizes using a different and more stable interface and contains a degenerate phosphothreonine-binding pocket. Our results suggest that the MU2 dimerization is constitutive and lacks phosphorylation-mediated regulation.

Structured summary of protein interactions:
MU2 and **MU2** bind by cosedimentation in solution (View interaction)
MU2 and **MU2** bind by X-ray crystallography (View interaction)
MU2 and **MU2** bind by molecular sieving (View interaction)

1. Introduction

DNA double-strand breaks (DSBs) produced by genotoxic agents and in normal cellular processes are highly harmful to genome stability. Eukaryotes employ sophisticated DNA damage responses (DDR) to detect DSBs, transduce their signal and repair them [1]. One of the earliest events upon induction of DSB is rapid phosphorylation of Ser139 near the C-terminus of the histone variant H2AX [2]. Phosphorylated H2AX (γH2AX) forms a platform on which a host of checkpoint and repair proteins assemble into discrete nuclear foci. Mediator of DNA damage checkpoint protein 1 (MDC1, also known as NFBD1) is a key mediator protein that organizes and maintains DNA damage foci in mammalian DDR [3–17].

MDC1 mediates multiple phosphorylation-dependent protein–protein interactions [18]. It is composed of an N-terminal forkhead-associated (FHA) domain, a long linker region harboring repetitive short SDT, TQXF and PST motifs, and a tandem BRCT domain at the C-terminus. The tandem BRCT domain binds phospho-Ser139 of γH2AX [7–9]. The TQXF motif is phosphorylated by ATM and binds the ubiquitin ligase RNF8 [11–13]. The SDT motif is constitutively phosphorylated at its serine and threonine residues by casein kinase 2 and recruits the Mre11–Rad50–NBS1 (MRN) complex via its interaction with NBS1 [14–17]. FHA domains are phosphothreonine (pThr) specific-binding domains that are widely present in DNA repair and checkpoint proteins [19]. The FHA domain of MDC1 has been reported to interact with CHK2, ATM and Rad51 [6,9,10]; however, the relevance of these interactions is unclear [18].

The MDC1 FHA domain was recently shown to form a dimer through asymmetric face-to-face β-sheet contacts [20–22]. The dimer interface is marginally stable by itself, but can be greatly strengthened by the intermolecular interaction of one FHA subunit with the phosphorylated threonine 4 (pThr4) at the N-terminus of the other FHA subunit in dimer [20,21]. The Thr4 residue is phosphorylated primarily by ATM in response to DNA damage, providing a mechanism that regulates MDC1 dimer formation and function [20,21]. It was reported that MDC1 Thr98 is phosphorylated by ATM, inducing MDC1 self-association [23]. However, this conclusion has been challenged since Thr98 is totally buried in the FHA structure and inaccessible to phosphorylation [20,21].

The MDC1 interacting partners γH2AX and the MRN complex are evolutionarily conserved from yeast to humans. However, no homologs of MDC1 are apparent in lower eukaryotes. Drosophila mutator 2 (MU2) has been proposed as the ortholog of MDC1 based on the similarities in sequence and function [24]. First, they share

Abbreviations: MU2, mutator 2; MDC1, mediator of DNA damage checkpoint protein 1; FHA, forkhead-associated; DDR, DNA damage response; DSB, double-strand break

* Corresponding author. Fax: +86 10 80728592.
E-mail address: yekeqiong@nibs.ac.cn (K. Ye).

0014-5793/$36.00
doi:10.1016/j.febslet.2012.01.023

similar domain architectures with an N-terminal FHA domain and a C-terminal tandem BRCT domain (Fig. 1A). Second, their tandem BRCT domains all bind γH2AX (γH2Av in Drosophila). MU2 likewise forms DNA damage foci that co-localize with γH2Av foci. Third, an N-terminal fragment of MU2 associates with the MRN complex. Fourth, MU2 has been genetically linked to DSB repair; a mutation in the *mu2* gene led to defects in DSB repair and an increased frequency of neotelomeres [24–27].

MU2 and MDC1 share only 10% sequence identity and 22% similarity in the FHA domain. It is unknown whether the dimerization function of the FHA domain is evolutionarily conserved in MU2. In this study, we determined the crystal structure of the MU2 FHA domain, revealing also a dimer. This identifies a new structural correspondence between MU2 and MDC1 and suggests a conserved role for FHA dimerization in MDC1/MU2 functions. However, the MU2 FHA dimer has a different dimer interface with higher intrinsic stability and a degenerate pThr-binding pocket as compared to the MDC1 FHA domain.

2. Materials and methods

2.1. Gene cloning and protein purification

The DNA sequence encoding residues 1–101 of MU2 (CG1960) was PCR amplified from a Drosophila cDNA clone obtained from the Drosophila Genomics Resource Center and cloned into a modified pET-28a + plasmid, in which the FHA domain was fused to the C-terminus of a His_6-SMT3 tag. The protein was expressed in the *Escherichia coli* BL21(DE3) strain (Novagen), which was induced with 0.2 mM IPTG overnight at 25 °C. The harvested cells were resuspended in buffer P500 (50 mM sodium phosphate pH 7.6, 500 mM NaCl) and lysed using a JN-3000 PLUS cell disrupter (JNBIO) and brief sonication. After clarification, the supernatant was loaded onto a 5-ml HisTrap column (GE Healthcare). The protein was eluted with 250 mM imidazole in buffer P500. The His_6-SMT3 tag was cleaved with His-tagged ULP1 protease at 4 °C for 0.5 h. After the imidazole concentration was lowered to 5 mM by repeated steps of concentration and dilution, the protein sample was passed over another HisTrap column to remove the cleaved tag, uncleaved protein and His-tagged ULP1. The cleaved MU2 FHA domain was collected from the flow-through and further purified with Superdex-75 16/60 column in 5 mM HEPES-K pH 7.6 and 100 mM KCl. The peak fractions were collected and concentrated to 25 mg/ml. All purification procedures were carried out at 4 °C.

2.2. Crystallization and data collection

MU2 (1–101) was crystallized by mixing 1 μl of protein sample (25 mg/ml, 5 mM HEPES-K pH 7.6 and 100 mM KCl) and 1 μl of well solution (0.2 M calcium acetate pH 7.5 and 18% PEG 3350)

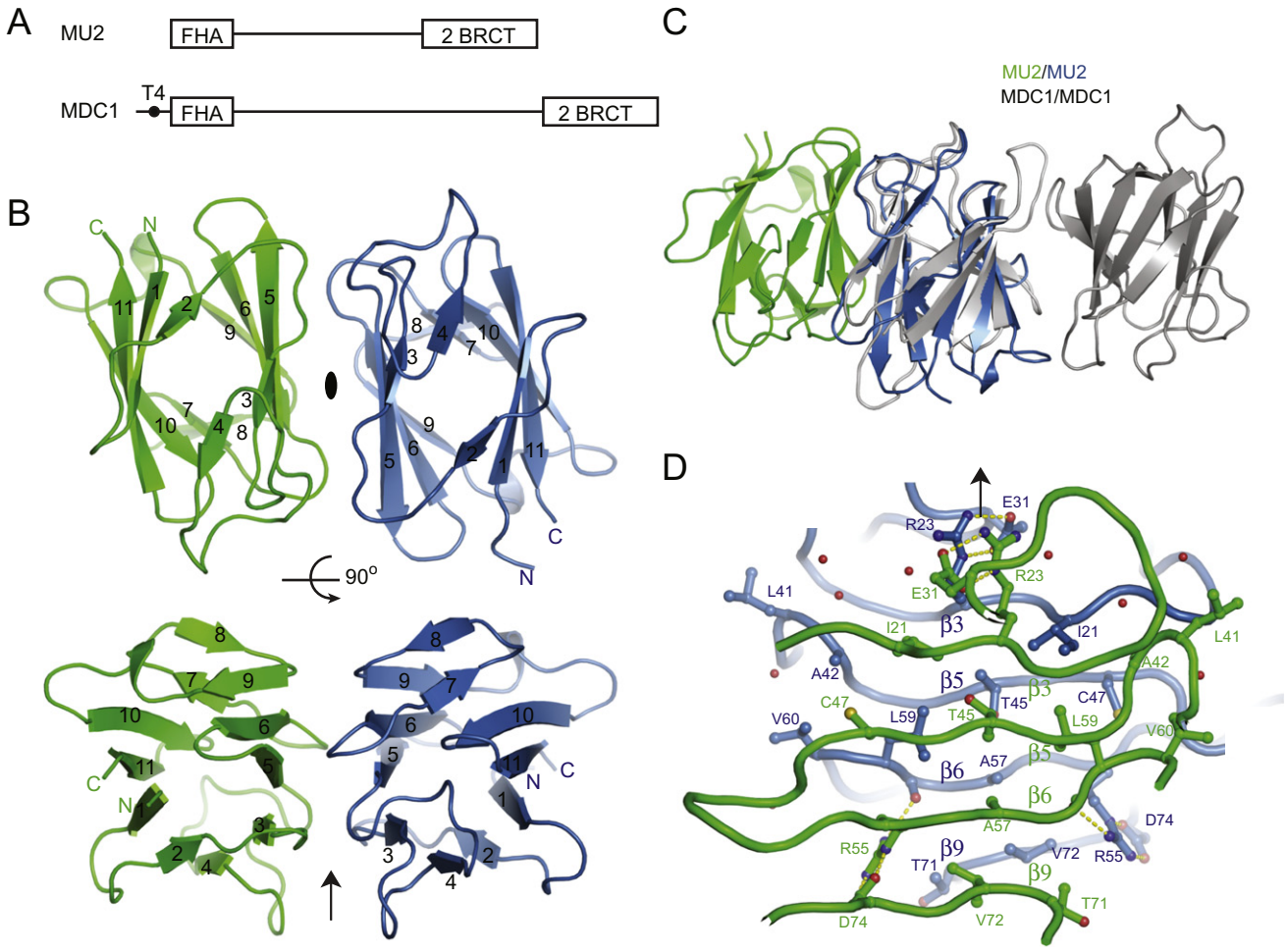

Fig. 1. Dimeric structure of the MU2 FHA domain. (A) Domain diagram of MU2 and MDC1. (B) Ribbon representation of the dimeric MU2 FHA structure. The two subunits are colored green and blue. Two orientations, which are viewed down and perpendicular to the dyad axis (ellipse and arrow), are shown. The β-strands and the N- and C-termini are labeled. (C) Structural superimposition of MU2 (green and blue) and MDC1 FHA dimer (gray) using one subunit. (D) Interactions at the dimer interface. Protein chains are shown as tubes, interacting residues as sticks, bridging water molecules as red spheres and hydrogen bonds as dashed lines. Carbon atoms are colored green in one subunit and blue in the other subunit, oxygen atoms are red and nitrogen atoms are blue.

using the hanging drop vapor diffusion approach at 4 °C. The initially obtained microcrystals were improved by microseeding and macroseeding in drops containing 1 μl of protein solution (10 mg/ml) and 1 μl of the well solution. Platinum derivatives were prepared by soaking crystals in the well solution containing 1 mM potassium tetrachloroplatinate for 5 h. Crystals were cryoprotected in 20% glycerol in the well solution prior to freezing in liquid nitrogen. Diffraction data for native and derivative crystals were collected at 100 K using a Rigaku machine at a wavelength of 1.5418 Å. A native dataset for the final refinement was collected at the Shanghai Synchrotron Research Facility beamline BL17U. Data were processed with Denzo/Scalepack or HKL2000 [28].

2.3. Structure determination and refinement

The crystals belong to space group $P6_5$ with two molecules of MU2 (1–101) in the asymmetric unit. The structure was determined by the single isomorphism replacement with anomalous scattering (SIRAS) method using native and derivative datasets. Heavy atom search, phase calculation and density modification were conducted with SHARP [29]. The model building and refinement were completed using AutoBuild in Phenix [30], Coot [31] and Refmac [32]. The model was refined to 1.9 Å and contained two MU2 FHA domains with residues 1–99 and 3–99 as well as 135 water molecules. In the Ramachandran plot, 97.4% of the residues are in favored region and 2.6% in allowed region. The structure figures were created using PyMOL [33]. The atomic coordinates and the structure factors of the MU2 FHA structure have been deposited in the Protein Data Bank under accession code 3UV0.

2.4. Gel filtration

The gel filtration experiments were conducted at 4 °C with a Superdex 75 10/300 column that was equilibrated in buffer P150 (50 mM sodium phosphate pH 7.6, 150 mM NaCl). The column was calibrated with bovine serum albumin (67 kD), ovalbumin (43 kD), chymotrypsinogen (25 kD), cytochrome C (12.4 kD) and aprotinin (6.5 kD). MU2 (1–101), MDC1 (27–138) and the L127R mutant of MDC1 (27–138) were loaded using 120 μl of each sample (350–500 μM).

2.5. Sedimentation equilibrium

The sedimentation equilibrium experiments were conducted using an XL-I analytical ultracentrifuge (Beckman Coulter) that was equipped with an An-60 Ti rotor and a six-channel centerpiece. The protein sample was exchanged to buffer P150 by gel filtration and loaded at a concentration of 67 μM. The protein was centrifuged at 25 °C at speeds of 25000, 30000 and 38000 rpm and detected using UV absorbance at 280 nm. The data were globally fitted as described previously [20].

3. Results

3.1. Dimeric structure of MU2 FHA

We cloned, expressed, purified and crystallized a MU2 fragment that contained residues 1–101. The structure was determined by SIRAS phasing using platinum derivative and native crystals and refined to 1.9 Å resolution with an R_{work}/R_{free} of 0.178/0.227 and excellent stereochemistry (Table 1). The structure adopts a typical FHA fold with 11 β-strands (β1–β11) forming a two-sheet β-sandwich (Fig. 1B) [34]. The β-sheet 1 is composed of 6 strands in the order β2–β1–β11–β10–β7–β8, whereas the β-sheet 2 is assembled by 5 strands in the order β4–β3–β5–β6–β9. The individual subunit structure of the MU2 FHA domain can be aligned to that of the MDC1 FHA domain with a root mean square deviation (RMSD) of 0.923 Å over 46 Cα pairs (Fig. 1C) [20].

In crystal, the two subunits contact each other via β-sheet 2, forming a symmetric homodimer. The strands β3, β5, β6 and β9 contact their counterparts in the other subunit in an antiparallel alignment. The dyad axis is roughly perpendicular to the running direction of these strands. The central area of the dimer interface is mainly hydrophobic and comprises the residues Ile21, Arg23 (aliphatic part), Leu41, Ala42, Thr45, Cys47, Arg55 (aliphatic part), Ala57, Leu59, Val60 and Val72 (Fig. 1D). In addition, on one side of the dimer interface, Arg55 forms a salt bridge to Glu74 from the same subunit and hydrogen bonds to the carbonyl oxygen atom of Ala58 in the other subunit. On the other side of the dimer interface, the planar guanidinium group of Arg23, which is stabilized by a salt bridge with Glu31 from the same subunit, stacks over its counterpart in the other subunit. Many water molecules were observed to mediate the indirect inter-subunit contacts.

The dimer interface buries a solvent-accessible area of 872 $Å^2$ for each subunit, accounting for 15.5% of total surface. Compared to other crystallographic contacts, this chosen interface is the most extensive: the next large interface covers an area of 488 $Å^2$. To verify the dimer interface observed in the crystal, we introduced a few single (T45R, L59R and I21R) and double mutations (T45R/L59R, T45R/I21R) into the dimer interface. However, each of these mutant proteins failed to be purified owing to severe aggregation problems, suggesting that these residues at the dimer interface are critical for the integrity of the structure.

Although the FHA domain of MDC1 and MU2 both form a dimer, their dimer interfaces are different from each other: the MDC1 FHA domain dimerizes via β-sheet 1, whereas the MU2 FHA domain dimerizes via the opposite β-sheet 2 (Fig. 1C). Moreover, the dimer interface is slightly asymmetric in the MDC1 FHA domain [20–22] but is symmetric in the MU2 FHA domain.

3.2. MU2 FHA forms a stable dimer in solution

To test whether the MU2 FHA domain forms a dimer also in solution, we analyzed its molecular size by gel filtration chromatography. The calculated apparent molecular weights were 27 kD for the MU2 FHA domain, 24 kD for the MDC1 FHA domain con-

Table 1
Data collection and refinement statistics.

Crystal form	Pt	Native
Data collection		
Space group	$P6_5$	$P6_5$
Cell dimensions		
a, *b*, *c* (Å)	100.2, 100.2, 38.2	99.9, 99.9, 38.3
α, β, γ (°)	90, 90, 120	90, 90, 120
Wavelength (Å)	1.5418	0.9796
X-ray source	Cu-K	SSRF BL17U
Resolution range (Å)	25–2.80 (2.85–2.80)	20–1.90 (1.93–1.90)
Unique reflections	5591	17,428
Redundancy	16.9 (12.0)	11.1 (7.6)
I/σ	16.7 (4.1)	24.8 (3.8)
Completeness (%)	100.0 (100.0)	98.6 (80.8)
R_{merge}	0.206 (0.665)	0.122 (0.391)
Structure refinement		
Resolution range (Å)		18.9–1.90 (1.95–1.90)
No. reflections		16,472 (1180)
No. atoms		1636
Mean B factor ($Å^2$)		18.2
R_{work}		0.178 (0.164)
R_{free}		0.227 (0.255)
RMSD bond length (Å)		0.015
RMSD bond angles (°)		1.591

Values for the data in the highest resolution bin are shown in parentheses.

taining residues 27–138 and 15 kD for the L127R monomer mutant of MDC1 (27–138) (Fig. 2A) [20]. These results demonstrate that the MU2 FHA domain behaved as a dimer in solution.

By analytic ultracentrifugation sedimentation equilibrium experiments, we showed that the MU2 FHA domain forms a highly stable dimer with an apparent dissociation constant K_d of 0.19 nM (Fig. 2B). By comparison, the MDC1 FHA dimer with unphosphorylated Thr4 is ~50000-fold less stable with a K_d value of 9.2 μM [20]. Notably, the MDC1 (27–138) dimer appeared smaller than the MU2 (1–101) dimer in gel filtration experiments. The MDC1 (27–138) dimer, which is weakly self-associated by itself, likely partially dissociated into monomers, resulting in a delayed and trailing peak in the elution profile (Fig. 2A). In contrast, the stable MU2 FHA dimer exhibited a symmetric elution peak, indicating a homogenous dimer population. The dramatic difference in stability between MU2 and MDC1 FHA dimers can be explained by the more extensive dimer interface in MU2 (872 Å^2) compared to that in MDC1 (490 Å^2) [20].

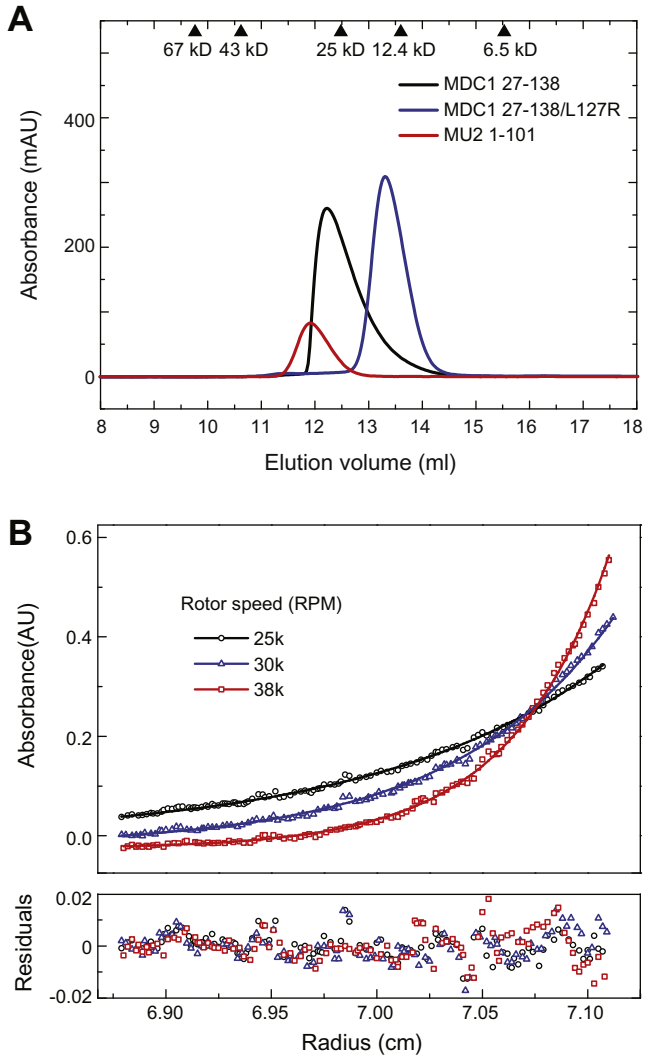

Fig. 2. The MU2 FHA domain forms a stable dimer in solution. (A) Size exclusion chromatography profiles of MU2 (1–101), MDC1 (27–138) and the L127R monomer mutant of MDC1 (27–138). Each sample (350–500 μM) were loaded in 120 μl to a Superdex 75 column. The elution positions of the calibration standards are indicated on the top. (B) Analytic ultracentrifugation sedimentation equilibrium analysis of the MU2 FHA domain. The lines show the best global fit to three profiles at spin speeds 25000, 30000 and 38000 rpm with a dimer dissociation constant K_d of 0.19 nM.

3.3. The MU2 FHA domain has a degenerate pThr-binding pocket

The pThr-binding pocket of FHA domain is situated at one end of the β-sandwich and is composed of three loops between the strands β3 and β4, β4 and β5 and β6 and β7 [13,34–44]. Although the corresponding pocket in the MU2 FHA domain is not occluded by dimerization, the pocket lacks three key residues for pThr binding (Fig. 3A and B). The first residue is an invariant serine residue (Ser72 in MDC1), which forms a hydrogen bond to the phosphate group of bound pThr. This serine residue is replaced by Glu40 in MU2 and the negatively charged side chain of Glu40 would repel the negatively charged phosphate group of pThr. The second residue is located at the immediate C-terminal side to the invariant serine and is frequently a positively charged lysine or arginine residue (Lys73 in MDC1) that neutralizes the negative charge of pThr phosphate. This position is occupied by Leu41 in MU2. The third residue is an asparagine residue (Asn96 in MDC1), which forms two hydrogen bonds with the backbone atoms of the bound phosphopeptide. The β6–β7 loop in the MU2 FHA domain is shorter by two residues compared to that in the MDC1 FHA domain, which causes an alternative conformation of the loop and the absence of this key asparagine residue. Nevertheless, an arginine residue (Arg26 in MU2 and Arg58 in MDC1) in the β3–β4 loop that contacts the phosphate group and the phosphopeptide backbone is preserved. These structural features of the pThr-binding pocket strongly suggest that the MU2 FHA domain lacks the capability of binding pThr. However, we cannot formally rule out the possibility that the MU2 FHA domain binds phosphopeptide in an unconventional way. Experimentally, we detected no binding of the MU2 FHA domain to a N-terminal pThr4 peptide of MDC1 using isothermal titration calorimetry (data not shown).

4. Discussion

We have shown that the FHA domain of MU2 plays an evolutionarily conserved role in dimerization. This finding extends the structural correspondence between MU2 and MDC1 to their FHA domains and supports that MU2 is the ortholog of MDC1. Nevertheless, MU2 and MDC1 FHA dimers show several marked structural differences. They dimerize via two opposite interfaces with different intrinsic stability. The MDC1 FHA domain binds to pThr4 from the other molecule in dimer and this *trans*-interaction is required for formation of a stable dimer [20,21]. By contrast, the MU2 FHA domain does not contain a functional pThr-binding pocket and an N-terminal tail that harbors a potential pThr site. The MU2 FHA domain forms a highly stable dimer by itself, which would obviate the need for additional intermolecular pThr-interaction to stabilize dimer formation and prevent any dimerization-dependent functional regulation. Hence, MU2 dimerization is constitutive in Drosophila, whereas MDC1 dimerization is regulated in mammals, which may contribute to the increased complexity in mammalian DDR. Our results show that dimerization, rather than pThr-binding, is conserved between the MU2 and MDC1 FHA domains.

The MDC1 FHA domain was reported to bind CHK2 and ATM through pThr-recognition [6,9]. These interactions should not be conserved in Drosophila MU2 since it has a defective pThr-binding pocket. A recombinant N-terminal fragment of MU2 (residues 1–250) was shown to bind the MRN complex [24]. The MU2–MRN interaction is also unlikely to occur through the conventional FHA-mediated recognition of pThr sites in the MRN complex. Alternatively, the MU2–MRN interaction is likely mediated by the MU2 FHA domain in a pThr-independent manner or by the C-terminal region of the FHA domain.

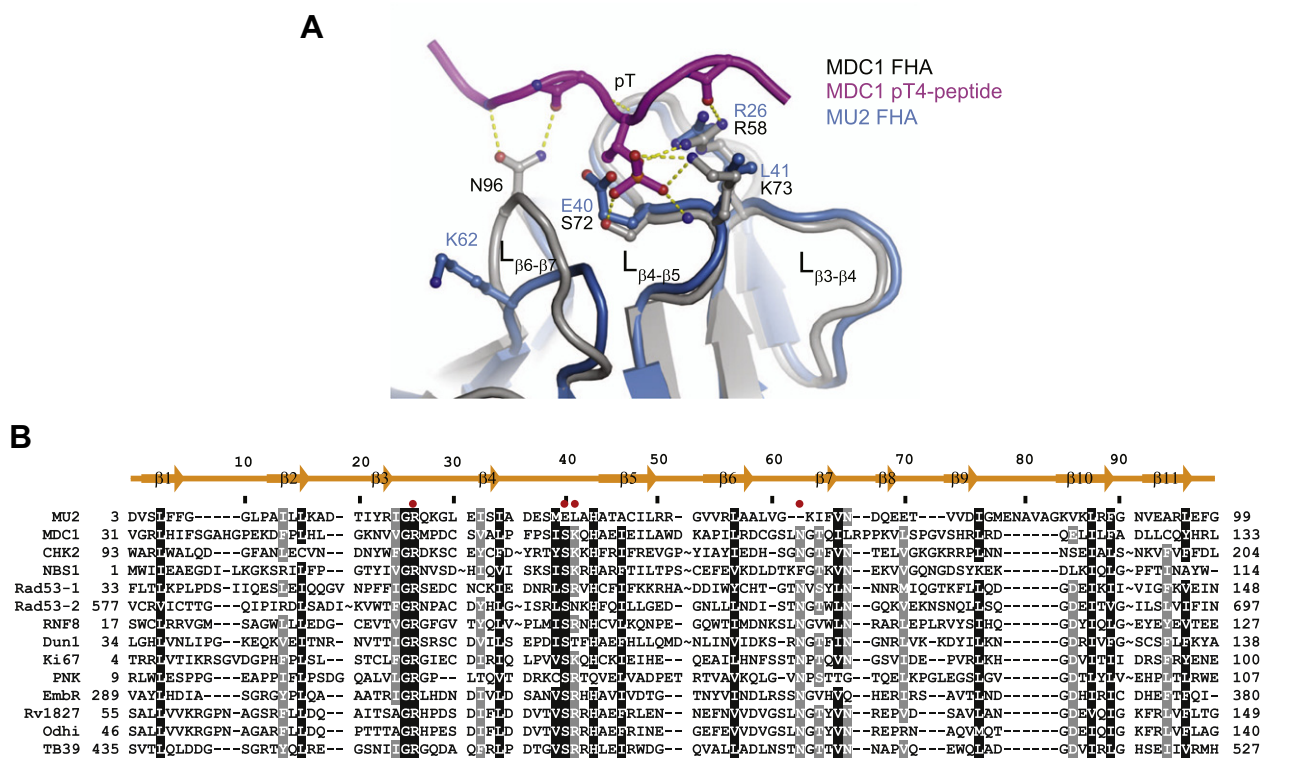

Fig. 3. The MU2 FHA domain contains a degenerate pThr-binding pocket. Superposition of the structure of the MU2 FHA domain with the monomeric structure of the MDC1 FHA domain in complex with a pThr4 phosphopeptide (PDB code: 3UNN). The phosphopeptide and important phosphopeptide-binding residues are shown in stick-and-ball representation and colored by atoms. (B) Structure based sequence alignment of the FHA domains of MU2, MDC1, CHK2 (PDB code: 1GXC) [42], NBS1 (3HUF) [36], Rad53 (first, 1G6G) [34], Rad53 (second, 1J4L) [43], RNF8 (2PIE) [13], Dun1 (2JQL) [39], Ki67 (2AFF) [41], PNK (2W3O) [38], EmbR (2FF4) [40], Rv1827 (2KFU) [37], Odhi (2KB3) [44] and TB39 (3POA) [35]. Phosphopeptide-binding residues are marked with solid cycles. The secondary structures and residue numbers are indicated for the MU2 FHA domain. Omitted residues are indicated by "∼". Residues that are conserved in 95% and 80% of these sequences are shaded in black and gray, respectively.

Acknowledgements

We thank the staff at the Shanghai Synchrotron Radiation Facility beamline BL17U for their assistance in diffraction data collection, Xiaoxia Yu at the Institute of Biophysics, Chinese Academy of Sciences, for the AUC experiments and Shanshan Wang for technical assistance. We also thank Drs. Li-Lin Du and Xingzhi Xu for stimulating discussion and comments. The research was supported by the Chinese Ministry of Science and Technology (863 project 2008AA022310 and 973 project 2010CB835402) and the Beijing Municipal Government.

References

[1] Ciccia, A. and Elledge, S.J. (2010) The DNA damage response: making it safe to play with knives. Mol. Cell 40, 179–204.
[2] Rogakou, E.P., Pilch, D.R., Orr, A.H., Ivanova, V.S. and Bonner, W.M. (1998) DNA double-stranded breaks induce histone H2AX phosphorylation on serine 139. J. Biol. Chem. 273, 5858–5868.
[3] Xu, X. and Stern, D.F. (2003) NFBD1/KIAA0170 is a chromatin-associated protein involved in DNA damage signaling pathways. J. Biol. Chem. 278, 8795–8803.
[4] Goldberg, M., Stucki, M., Falck, J., D'Amours, D., Rahman, D., Pappin, D., Bartek, J. and Jackson, S.P. (2003) MDC1 is required for the intra-S-phase DNA damage checkpoint. Nature 421, 952–956.
[5] Stewart, G.S., Wang, B., Bignell, C.R., Taylor, A.M. and Elledge, S.J. (2003) MDC1 is a mediator of the mammalian DNA damage checkpoint. Nature 421, 961–966.
[6] Lou, Z., Minter-Dykhouse, K., Wu, X. and Chen, J. (2003) MDC1 is coupled to activated CHK2 in mammalian DNA damage response pathways. Nature 421, 957–961.
[7] Stucki, M., Clapperton, J.A., Mohammad, D., Yaffe, M.B., Smerdon, S.J. and Jackson, S.P. (2005) MDC1 directly binds phosphorylated histone H2AX to regulate cellular responses to DNA double-strand breaks. Cell 123, 1213–1226.
[8] Lee, M.S., Edwards, R.A., Thede, G.L. and Glover, J.N. (2005) Structure of the BRCT repeat domain of MDC1 and its specificity for the free COOH-terminal end of the gamma-H2AX histone tail. J. Biol. Chem. 280, 32053–32056.
[9] Lou, Z. et al. (2006) MDC1 maintains genomic stability by participating in the amplification of ATM-dependent DNA damage signals. Mol. Cell 21, 187–200.
[10] Zhang, J., Ma, Z., Treszezamsky, A. and Powell, S.N. (2005) MDC1 interacts with Rad51 and facilitates homologous recombination. Nat. Struct. Mol. Biol. 12, 902–909.
[11] Mailand, N., Bekker-Jensen, S., Faustrup, H., Melander, F., Bartek, J., Lukas, C. and Lukas, J. (2007) RNF8 ubiquitylates histones at DNA double-strand breaks and promotes assembly of repair proteins. Cell 131, 887–900.
[12] Kolas, N.K. et al. (2007) Orchestration of the DNA-damage response by the RNF8 ubiquitin ligase. Science 318, 1637–1640.
[13] Huen, M.S., Grant, R., Manke, I., Minn, K., Yu, X., Yaffe, M.B. and Chen, J. (2007) RNF8 transduces the DNA-damage signal via histone ubiquitylation and checkpoint protein assembly. Cell 131, 901–914.
[14] Spycher, C., Miller, E.S., Townsend, K., Pavic, L., Morrice, N.A., Janscak, P., Stewart, G.S. and Stucki, M. (2008) Constitutive phosphorylation of MDC1 physically links the MRE11-RAD50-NBS1 complex to damaged chromatin. J. Cell Biol. 181, 227–240.
[15] Wu, L., Luo, K., Lou, Z. and Chen, J. (2008) MDC1 regulates intra-S-phase checkpoint by targeting NBS1 to DNA double-strand breaks. Proc. Natl. Acad. Sci. USA 105, 11200–11205.
[16] Melander, F., Bekker-Jensen, S., Falck, J., Bartek, J., Mailand, N. and Lukas, J. (2008) Phosphorylation of SDT repeats in the MDC1 N terminus triggers retention of NBS1 at the DNA damage-modified chromatin. J. Cell Biol. 181, 213–226.
[17] Chapman, J.R. and Jackson, S.P. (2008) Phospho-dependent interactions between NBS1 and MDC1 mediate chromatin retention of the MRN complex at sites of DNA damage. EMBO Rep. 9, 795–801.
[18] Jungmichel, S. and Stucki, M. (2010) MDC1: the art of keeping things in focus. Chromosoma 119, 337–349.
[19] Mohammad, D.H. and Yaffe, M.B. (2009) 14-3-3 proteins, FHA domains and BRCT domains in the DNA damage response. DNA Repair (Amst) 8, 1009–1017.
[20] Liu, J., Luo, S., Zhao, H., Liao, J., Li, J., Yang, C., Xu, B., Stern, D.F., Xu, X. and Ye, K. (2012) Structural mechanism of the phosphorylation-dependent dimerization of the MDC1 forkhead-associated domain. Nucleic Acids Res., doi:10.1093/nar/gkr1296.

[21] Jungmichel, S. et al. (2012) The molecular basis of ATM-dependent dimerization of the Mdc1 DNA damage checkpoint mediator. Nucleic Acids Res., doi:10.1093/nar/gkr1300.
[22] Wu, H.H., Wu, P.Y., Huang, K.F., Kao, Y.Y. and Tsai, M.D. (2012) Structural delineation of MDC1-FHA domain binding with CHK2-pThr68. Biochemistry, doi:10.1021/bi201709w.
[23] Luo, K., Yuan, J. and Lou, Z. (2011) Oligomerization of MDC1 protein is important for proper DNA damage response. J. Biol. Chem. 286, 28192–28199.
[24] Dronamraju, R. and Mason, J.M. (2009) Recognition of double strand breaks by a mutator protein (MU2) in *Drosophila melanogaster*. PLoS Genet. 5, e1000473.
[25] Mason, J.M., Strobel, E. and Green, M.M. (1984) Mu-2: mutator gene in Drosophila that potentiates the induction of terminal deficiencies. Proc. Natl. Acad. Sci. USA 81, 6090–6094.
[26] Kasravi, A., Walter, M.F., Brand, S., Mason, J.M. and Biessmann, H. (1999) Molecular cloning and tissue-specific expression of the mutator2 gene (mu2) in *Drosophila melanogaster*. Genetics 152, 1025–1035.
[27] Mason, J.M., Champion, L.E. and Hook, G. (1997) Germ-line effects of a mutator, mu2, in *Drosophila melanogaster*. Genetics 146, 1381–1397.
[28] Otwinowski, Z. and Minor, W. (1997) Processing of X-ray diffraction data collected in oscillation mode. Methods Enzymol. 276, 307–326.
[29] Vonrhein, C., Blanc, E., Roversi, P. and Bricogne, G. (2007) Automated structure solution with autoSHARP. Methods Mol. Biol. 364, 215–230.
[30] Adams, P.D. et al. (2010) PHENIX: a comprehensive Python-based system for macromolecular structure solution. Acta Crystallogr. D Biol. Crystallogr. 66, 213–221.
[31] Emsley, P. and Cowtan, K. (2004) Coot: model-building tools for molecular graphics. Acta Crystallogr. D Biol. Crystallogr. 60, 2126–2132.
[32] Murshudov, G.N., Vagin, A.A., Lebedev, A., Wilson, K.S. and Dodson, E.J. (1999) Efficient anisotropic refinement of macromolecular structures using FFT. Acta Crystallogr. D Biol. Crystallogr. 55, 247–255.
[33] DeLano, W.L. (2002) The PyMOL user's manual, Delano Scientific, San Carlos, CA, USA.
[34] Durocher, D., Taylor, I.A., Sarbassova, D., Haire, L.F., Westcott, S.L., Jackson, S.P., Smerdon, S.J. and Yaffe, M.B. (2000) The molecular basis of FHA domain:phosphopeptide binding specificity and implications for phospho-dependent signaling mechanisms. Mol. Cell 6, 1169–1182.
[35] Pennell, S. et al. (2010) Structural and functional analysis of phosphothreonine-dependent FHA domain interactions. Structure 18, 1587–1595.
[36] Williams, R.S. et al. (2009) Nbs1 flexibly tethers Ctp1 and Mre11-Rad50 to coordinate DNA double-strand break processing and repair. Cell 139, 87–99.
[37] Nott, T.J. et al. (2009) An intramolecular switch regulates phosphoindependent FHA domain interactions in *Mycobacterium tuberculosis*. Sci. Signal. 2, ra12.
[38] Ali, A.A., Jukes, R.M., Pearl, L.H. and Oliver, A.W. (2009) Specific recognition of a multiply phosphorylated motif in the DNA repair scaffold XRCC1 by the FHA domain of human PNK. Nucleic Acids Res. 37, 1701–1712.
[39] Lee, H., Yuan, C., Hammet, A., Mahajan, A., Chen, E.S., Wu, M.R., Su, M.I., Heierhorst, J. and Tsai, M.D. (2008) Diphosphothreonine-specific interaction between an SQ/TQ cluster and an FHA domain in the Rad53-Dun1 kinase cascade. Mol. Cell 30, 767–778.
[40] Alderwick, L.J., Molle, V., Kremer, L., Cozzone, A.J., Dafforn, T.R., Besra, G.S. and Futterer, K. (2006) Molecular structure of EmbR, a response element of Ser/Thr kinase signaling in *Mycobacterium tuberculosis*. Proc. Natl. Acad. Sci. USA 103, 2558–2563.
[41] Byeon, I.J., Li, H., Song, H., Gronenborn, A.M. and Tsai, M.D. (2005) Sequential phosphorylation and multisite interactions characterize specific target recognition by the FHA domain of Ki67. Nat. Struct. Mol. Biol. 12, 987–993.
[42] Li, J., Williams, B.L., Haire, L.F., Goldberg, M., Wilker, E., Durocher, D., Yaffe, M.B., Jackson, S.P. and Smerdon, S.J. (2002) Structural and functional versatility of the FHA domain in DNA-damage signaling by the tumor suppressor kinase Chk2. Mol. Cell 9, 1045–1054.
[43] Byeon, I.J., Yongkiettrakul, S. and Tsai, M.D. (2001) Solution structure of the yeast Rad53 FHA2 complexed with a phosphothreonine peptide pTXXL: comparison with the structures of FHA2-pYXL and FHA1-pTXXD complexes. J. Mol. Biol. 314, 577–588.
[44] Barthe, P., Roumestand, C., Canova, M.J., Kremer, L., Hurard, C., Molle, V. and Cohen-Gonsaud, M. (2009) Dynamic and structural characterization of a bacterial FHA protein reveals a new autoinhibition mechanism. Structure 17, 568–578.